

# Revealing the spiral arms through radial migration and the shape of the Metallicity Distribution Function

L.A. Martinez-Medina <sup>\*</sup>, B. Pichardo, E. Moreno, & A. Peimbert

*Instituto de Astronomía, Universidad Nacional Autónoma de México, A.P. 70–264, 04510, México, CDMX, Mexico*

9 August 2016

## ABSTRACT

Recent observations show that the Milky Way’s metallicity distribution function (MDF) changes its shape as a function of radius. This new evidence of radial migration within the stellar disc sets additional constraints on Galactic models. By performing controlled test particle simulations in a very detailed, observationally motivated model of the Milky Way, we demonstrate that, in the inner region of the disc, the MDF is shaped by the joint action of the bar and spiral arms, while at outer radii the MDF is mainly shaped by the spiral arms. We show that the spiral arms are able to imprint their signature in the radial migration, shaping the MDF in the outskirts of the Galactic disc with a minimal participation of the bar. Conversely, this work has the potential to characterise some structural and dynamical parameters of the spiral arms based on radial migration and the shape of the MDF. Finally, the resemblance obtained with this approximation to the MDF curves of the Galaxy as seen by APOGEE, show that a fundamental factor influencing their shape is the Galactic potential.

**Key words:** Galaxy: disc — Galaxy: evolution — Galaxy: kinematics and dynamics — Galaxy: structure

## 1 INTRODUCTION

An enormous effort has been dedicated, in the last decade, to the understanding of radial and vertical orbital stellar motions induced by the non-axisymmetric structures in the Galaxy (Sellwood & Binney 2002; Roškar et al. 2008; Grand et al. 2012a; Bird et al. 2012; Roškar et al. 2012; Vera-Ciro et al. 2014; Halle et al. 2015; Aumer et al. 2016, and references therein). Particular attention has been paid to stellar migration and its effects on the chemical elements distribution in the Galaxy (Schönrich & Binney 2009; Minchev et al. 2011, 2013, 2014; Sánchez-Blázquez et al. 2014; Hayden et al. 2015; Loebman et al. 2016).

The mechanism of radial migration, as defined by Sellwood & Binney (2002, hereafter SB02), is understood as the redistribution of angular momentum for stars that interact with the non-axisymmetric structure of the galaxy around the corotation resonance while keeping their orbital eccentricity unchanged. On the other hand, redistribution of angular momentum at radii different from corotation will cause a dynamical heating of the stellar disc. Both mechanisms move stars to inner or outer radii, but radial migration does not leave a kinematic imprint on stellar orbits. It is worth noting that the term radial migration has been

used differently by different authors <sup>1</sup> (see for example the discussion by Vera-Ciro et al. 2014).

Without the effect of stellar migration, a perfect correlation between age and metallicity of a star could be found for a given Galactic region, assuming the abundance of chemical elements was known in such region. Although this seems to approximate the case for the ISM in the Milky Way (MW) and other galaxies (Wilson & Rood 1994; Henry & Worthey 1999), it is known that, for example, in the solar neighbourhood, stars of a given age show a large dispersion in metallicity (Edvardsson et al. 1993). This effect is not readily explained by plain orbital excursions from epicycles corresponding at their birth place (SB02).

More recently, Hayden et al. (2015), measure the metallicity distribution functions (MDFs) of the MW, from a sample of 69,919 red giants from the SDSS-III/APOGEE Data Release 12. They find that the shape of the midplane MDF changes systematically with radius, with a negatively skewed distribution at  $3 < R < 7$  kpc, to a roughly Gaussian distribution at the solar annulus, to a positively skewed shape in the outer Galaxy. Using a simple model they suggest that the reversal of MDF shape could be due to radial migration. However, a more complex model is needed to differentiate

<sup>\*</sup> Contact e-mail: lamartinez@astro.unam.mx

<sup>1</sup> The results presented in this paper do not depend on the specific definition of radial migration.

between the contribution of the different non-axisymmetric components of the Galaxy.

With detailed orbital studies performed in suitable observationally motivated potentials of the MW, we show here that the spiral arms can imprint their mark on the MDF.

This paper is organised as follows. The galactic model, initial conditions, and methodology are described in Section 2. A study on radial migration and radial heating is presented on Section 3. The link between the MDF and the initial radial distribution is shown in Section 4. Finally we present the discussion and conclusions, in Sections 5 and 6

## 2 THE GALAXY MODEL, NUMERICAL SIMULATIONS AND INITIAL CONDITIONS

A good numerical approach to study radial migration and its relation to MDFs in a Milky-Way sized N-body simulation was recently provided by [Loebman et al. \(2016\)](#). N-body simulations are not suitable to achieve the goals of this work, as we explain below. We employ instead a very detailed steady model adjusted specifically to the MW to the best of recent knowledge of the Galaxy structural and dynamical parameters (i.e. spiral arms and bar masses, density laws, scale-lengths, angular velocities, etc.).

We have selected this elaborate but steady model over a sophisticated N-body simulation (without resorting to the more common and simplistic cosine potential for the spiral arms with a Ferrers bar) for the following reasons:

1) The model is fully adjustable. We are able to fit the whole axisymmetric and non-axisymmetric potential (i.e. spiral arms and bar), in three dimensions to our best understanding of the Milky Way (or any other particular galaxy) from observations and models.

2) Rather than using a simple ad hoc model for a spiral perturbation, we employ a three-dimensional (3D) mass distribution for the spiral arms, from which we derive their gravitational potential and force fields. Our model is considerably faster, computationally speaking, than N-body simulations.

3) It allows us to study in great detail individual stellar orbital behaviour (e.g. resonant regions, vertical structure, chaotic and ordered behaviour, periodic orbits to estimate at some degree orbital self-consistency, etc.), without the resolution problems of N-body simulations.

We have integrated test particle orbits in this 3D Galactic potential model. Our model is observationally motivated by the MW and suitable to explain several characteristics of the local kinematics due to the spiral arms and the bar (such as moving groups in the solar neighbourhood, e.g. [Antoja et al. \(2009\)](#)).

Although the one employed is a much better suited spiral model to represent the Milky Way than any N-body simulation, we do not include any prescription of metallicity or ISM physics as in [Loebman et al. \(2016\)](#). In a future work, we will perform a more specific study of the spiral arms parameters, as well as implementing a metallicity prescription, to seek for a better fit to the APOGEE MDFs for the Milky Way Galaxy, and search for some restrictions to the morphology and physical characteristics of the spiral arms.

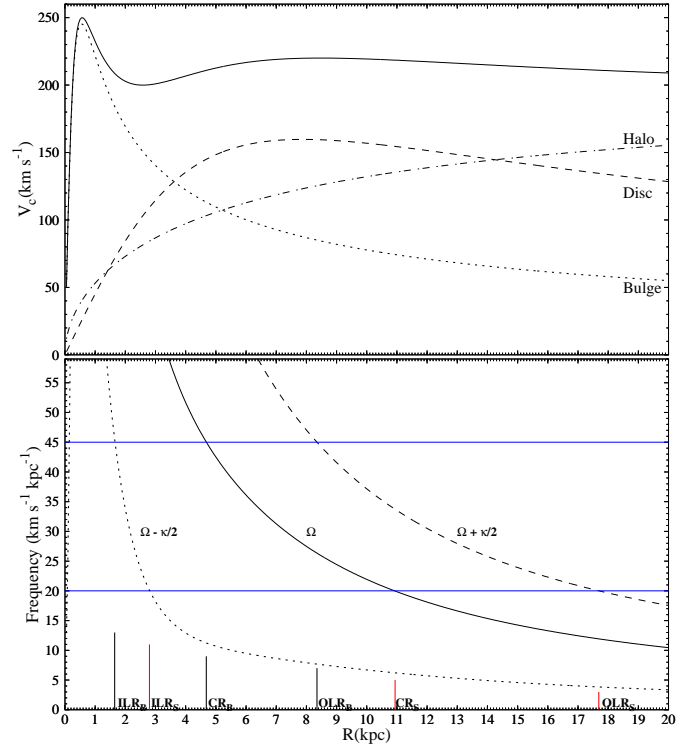


**Figure 1.** Top: Circular velocity for the bulge, disc, halo, and the full axisymmetric component of the model. Bottom: Frequencies diagram of the model. The vertical lines indicate the position of the inner and outer Lindblad resonances (ILR, OLR) and corotation (CR) for both the bar (black) and spiral arms (red). The horizontal blue lines represent the pattern speed of the bar ( $45 \text{ km s}^{-1} \text{ kpc}^{-1}$ ) and the spiral arms ( $20 \text{ km s}^{-1} \text{ kpc}^{-1}$ ).

### 2.1 The full Galactic model

The Galactic model is based on an axisymmetric model with the addition of non-axisymmetric components (spiral arms and bar). The axisymmetric galactic potential is based on the potential of [Allen & Santillán \(1991\)](#), that consists of a disc, a spherical bulge, and a supermassive spherical halo. All the mass of the spherical bulge is used to build the Galactic bar (see Section 2.3), likewise, the 3D spiral arms (see Section 2.2) are introduced by reducing the mass of the disc. At the beginning of each run, both structures are introduced slowly to diminish transients, by increasing their masses, as the bulge and disc masses are reduced. Finally, the Galactic potential is scaled to the Sun's galactocentric distance,  $R_0 = 8.5 \text{ kpc}$ , and the local rotation velocity,  $\Theta_0 = 220 \text{ km s}^{-1}$ . The rotation curve and frequencies diagram with the correspondent resonances are indicated in Figure 1.

### 2.2 The spiral arms

Numerous observational papers based on the younger components of the Galactic disc (HII regions, O-B stars, CO emission, masers in high-mass star-forming regions) show a four-armed spiral large scale structure in the Galaxy. On the other hand, observations in infrared bands such as those of the COBE/DIRBE K-band and the infrared Spitzer/GLIMPSE survey, show that only two of the

observed arms seem dominant (Drimmel & Spergel 2001; Churchwell et al. 2009). Based on models that have shown that two additional gaseous arms can be formed (without increasing the stellar surface density) as a response to a two-armed dominant pattern (Martos et al. 2004), in this work we will adopt a two-armed structure for the spiral arms.

For the spiral arms we employ the PERLAS model of Pichardo et al. (2003). The model is formed by a two-armed 3D density distribution made of individual inhomogeneous oblate spheroids. The spheroids act as bricks in a building, to construct the arms structure; they are located along a logarithmic spiral locus. PERLAS is completely adjustable (i.e. the width, height, scale lengths, density fall along the spiral arms and transversal to them, etc.) to better represent the available observations.

Our spiral arms simulate the main Galactic spiral arms based on the Spitzer/GLIMPSE database (Benjamin et al. 2005; Churchwell et al. 2009). The density is distributed as an exponential decline along the arms. The total mass of the spiral arms taken in these experiments is  $4.28 \times 10^9 M_\odot$ , that corresponds to a mass ratio of  $M_{\text{arms}}/M_{\text{disc}} = 0.05$ .

We employ the function  $Q_T$  (Sanders & Tubbs 1980; Combes & Sanders 1981) to measure the strength of the arms (which is proportional to their total mass). The maximum value of the function  $Q_T$  over the radial extent of the spiral arms (known as  $Q_s$ ) is calculated. The value obtained for  $Q_s$  is smaller than 0.25, which is in agreement with Buta et al. (2005), that finds that, for a galaxy like the Milky Way (Sbc),  $Q_s$  is approximately 0.25.

Finally, for the angular velocity, we use a value of  $\Omega_S = 20 \text{ km s}^{-1} \text{ kpc}^{-1}$ , provided by different observational and theoretical methods (see Gerhard (2011) for a review).

### 2.2.1 Transient spiral arms

There is no consensus in the astronomical community on the nature of spiral arms: fixed grand design vs transient and dynamic spirals. While some competent N-body simulations have shown long-lasting spiral arms (e.g. Saha & Elmegreen 2016), the most of them seem to show spiral arms as structures of transient nature (Hockney & Brownrigg 1974; Sellwood & Carlberg 1984; Roškar et al. 2008; Agertz et al. 2011; Sellwood & Carlberg 2014).

We have made an effort to consider the likely possibility that real galaxies have transient spiral arms. To this purpose, we introduce gradual changes in amplitude and angular speed in the arms. Note that, although we are not changing the pitch angle directly, by changing the amplitude we can represent changes not only to the mass but also mimic the effect of changing the pitch angle, which itself directly impacts the azimuthal forcing.

The construction of transient arms uses a simple assumption: the amplitude (equivalently the mass) of the spiral arms changes with a given periodicity. In this way the mass of the arms in the model can be made to depend explicitly on time, for which we have chosen the following time dependence:

$$M_s(t) = M_{\text{max}} |\sin(\pi t/t_l)|^f, \quad (1)$$

where  $M_s$  is the mass of the spiral pattern,  $t_l$  is the lifetime of each pattern (set to 1 Gyr),  $M_{\text{max}}$  is the maximum

value of the arms' mass during its lifetime, and the parameter  $f$  (set to 0.5) controls the flatness of each ripple in a plot of  $M_s(t)$ , i.e., it controls how long the mass remains nearly quiescent, and how fast  $M_s$  grows and diminishes outside the quiescent period. Similarly, to mimic a changing pattern speed we implemented a time dependent rotation frequency  $\Omega(t)$ . Although not conclusive, it seems from some N-body simulations, that new born spiral arms tend to decrease their angular speeds (Sellwood 2011). As a first approximation we set the rotation frequency of the initial pattern in the simulation to  $25 \text{ km s}^{-1} \text{ kpc}^{-1}$  and decreased it with each new pattern, to a minimum of  $17 \text{ km s}^{-1} \text{ kpc}^{-1}$ , at the end of the simulation. Since a functional form of  $\Omega(t)$  is not evident from N-body simulations, a simple assumption is that  $\Omega$  is constant during each time period  $t_i$ , in this way the adopted functional expression for  $\Omega(t)$  is a uniformly decreasing step function, each step indicates the value of the pattern speed for each short-lived spiral. We are aware that there is evidence of a more general relation for the pattern speed in N-body/dynamic spirals, that traces the material rotation frequency (See Rautiainen & Salo 1999; Baba et al. 2013; Roca-Fàbrega et al. 2013; Mata-Chávez et al. 2014; Pettitt et al. 2015; Grand et al. 2012b); in a future work we will study the dynamical effects of this specific characteristic of the spiral arms implemented on potential-particle models of the Galaxy.

As stated above, with the transiency implemented in this way, the main goal is not to reproduce all the features of dynamical spirals, but to test the impact of a time changing amplitude and pattern speed on the mechanism of radial migration, which is predicted be sensitive to both features.

### 2.3 The bar

For the bar we have selected the triaxial bar model of Pichardo et al. (2004); this is an inhomogeneous ellipsoid built as a the superposition of a large number of homogeneous ellipsoids to achieve a smooth density fall. The model approximates the density fall fitted by Freudreich (1998) from the COBE/DIRBE observations of the Galactic centre. The total mass of the bar is  $1.4 \times 10^{10} M_\odot$ , within the observational limits (e.g., Kent 1992; Zhao 1994; Dwek et al. 1995; Blum 1995; Stanek et al. 1997; Weiner & Sellwood 1999; Antoja et al. 2014). Regarding the angular speed, a long list of studies have estimated this parameter (Gerhard 2011, and references therein), concluding that the most likely value lies in the range  $\Omega_B = 45 - 60 \text{ km s}^{-1} \text{ kpc}^{-1}$ . For our computations, we adopt the value  $\Omega_B = 45 \text{ km s}^{-1} \text{ kpc}^{-1}$ , based on the formation of moving groups in the solar neighbourhood (Antoja et al. 2009).

A brief description of the observational/theoretical parameters utilised to model the bar and spiral arms is summarised in Table 1. For more specific details on the construction and our fit to observations see Martinez-Medina et al. (2015); Pichardo et al. (2004, 2003); Moreno et al. (2015); Pichardo et al. (2012).

### 2.4 Initial conditions

The initial distribution of test particles follows a Miyamoto-Nagai density profile discretised in  $10^6$  particles; the parti-

**Table 1.** Parameters of the non-axisymmetric Galactic components

Parameter	Value	Reference
<i>Triaxial ellipsoidal Bar</i>		
Major Semi-Axis	3.5 kpc	1
Scale Lengths	1.7, 0.64, 0.44 kpc	1
Axial Ratios	0.64/1.7, 0.44/1.7	1
Mass	$1.4 \times 10^{10} M_{\odot}$	2,3,4,5,6
Pattern Speed ( $\Omega_B$ )	45,20 km s <sup>-1</sup> kpc <sup>-1</sup>	7,8
<i>Spiral Arms</i>		
Number of spiral arms	2	9,10
Pitch Angle ( $i$ )	15.5°	11
Radial Scale Length ( $H_{\star}$ )	3 kpc	12
$M_{\text{arms}}/M_{\text{disc}}$	0.05	13
Mass	$4.28 \times 10^9 M_{\odot}$	13
Pattern Speed ( $\Omega_S$ )	20 km s <sup>-1</sup> kpc <sup>-1</sup>	8
$R_0$	8.5 kpc	

(1) [Freudenreich \(1998\)](#); (2) [Gerhard \(2002\)](#); (3) [Calchi Novati et al. \(2008\)](#); (4) [Zhao \(1996\)](#); (5) [Blum \(1995\)](#); (6) [Dwek et al. \(1995\)](#); (7) [Antoja et al. \(2014\)](#); (8) [Gerhard \(2011\)](#); (9) [Drimmel & Spergel \(2001\)](#); (10) [Churchwell et al. \(2009\)](#); (11) [Drimmel \(2000\)](#); (12) [Benjamin et al. \(2005\)](#); (13) [Pichardo et al. \(2003\)](#).

cles are distributed in the velocity space following the strategy of [Hernquist \(1993\)](#). When tested, the velocity dispersion does not evolve in the presence of the axisymmetric part of the model. Once the initial particle disc is constructed, the bar and spiral arms grow adiabatically for a time  $t_0$ , after which the mass of each component remains fixed. We follow a smooth function to grow the non-axisymmetric structures provided in equation 4 of [Dehnen \(2000\)](#) that avoids any sudden relaxation of the disc.

The mass of the spiral arms is given as a fraction of the mass of the disc and the mass of the bar is taken from the mass of the axisymmetric bulge. This means that, starting with the axisymmetric components of the model at time  $t = 0$ , during the time interval  $0 < t < t_0$ , a fraction of the disc mass is transferred to the arms and all the mass of the bulge is transferred to the bar.

A thorough test of the disc heating, measured from radial and vertical velocity dispersions, led us to take  $t_0 = 0.5$  Gyr as enough time to guarantee the absence of artificial effects in the simulations (i.e. heating).

The transient spiral arms are introduced adiabatically, as we do with the bar and the steady arms; the growing time for these experiments is 0.5 Gyr. Once the arms reach their maximum mass, the functional form of equation 1 will take place to mimic transiency by decreasing and increasing the mass of the spiral pattern. Notice that this functional dependence is not as smooth as our adiabatic growth (with this function we are trying to reproduce the behaviour seen, in general, in N-body simulations).

### 3 RADIAL MIGRATION AND RADIAL HEATING

The first aim of this work is to isolate the contributions of the spiral arms and of the central bar, in the context of

stellar radial migration, and then to compare them to the full Galactic model.

#### 3.1 Radial migration by the spiral arms

For the first MW model, the only non-axisymmetric component we consider is that of the spiral arms. We measure radial migration and heating in terms of changes in angular momentum calculated for each particle in the simulation during the period of time,  $\Delta t = t_f - t_i = 1$  Gyr, where the initial time,  $t_i = 4$  Gyr, and the final time,  $t_f = 5$  Gyr.

In the upper left panel of Figure 2, we present the change in angular momentum,  $\Delta L_z$ , for each particle as a function of the initial radii,  $R_i$ , in the time interval,  $\Delta t$ . The resonance locations of the spiral pattern are indicated in the figure. Note that all clear changes in angular momentum are linked to resonances. The theory predicts that changes that occur around the inner and outer Lindblad resonances are related to radial heating of the stellar disc, while  $\Delta L_z$  occurring at corotation, are mainly related to radial migration (SB02).

To test this prediction, in the lower left panel of Figure 2 we present the changes in orbital eccentricity within the same period of time,  $\Delta t$ , as a function of the initial radii. It can be seen that the gains and losses of angular momentum around the ILR correspond to changes in the orbital eccentricity (i.e. radial heating). On the other hand the gains and losses of angular momentum around CR are similar in magnitude to what happens around the ILR, but show a very different kinematic behaviour: in corotation the changes in the orbital eccentricity are much smaller than in the ILR, indicating the presence of radial migration.



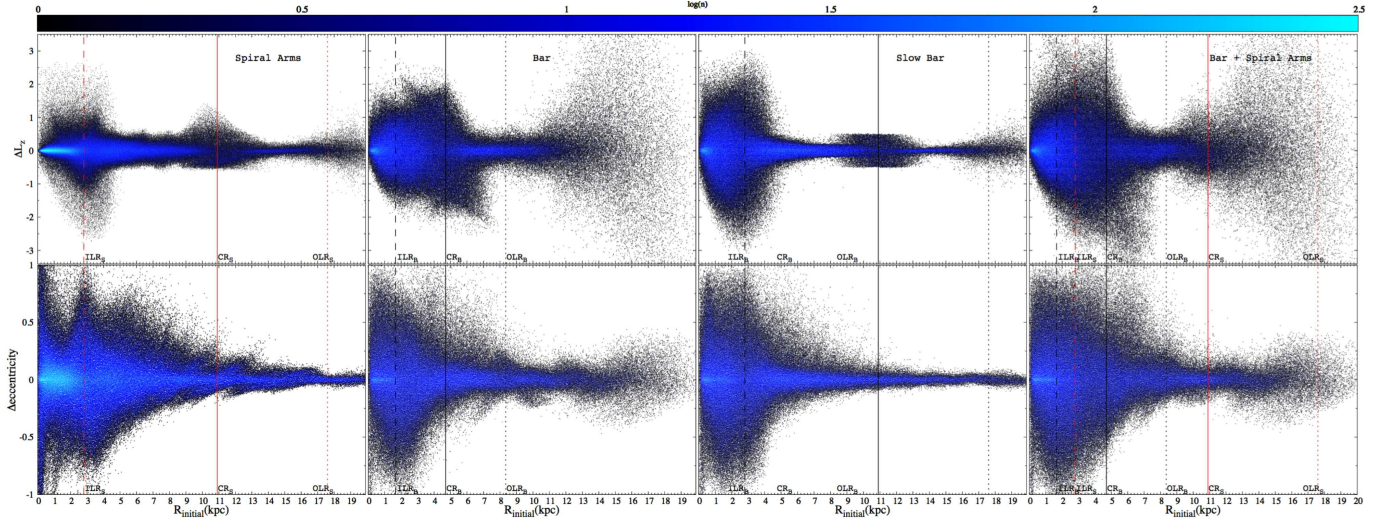


**Figure 2.** Changes in angular momentum (top row) and changes in eccentricity (bottom row), both as a function of the initial radius  $R_i$ . First column: simulation with spiral arms + axisymmetric potential. Second column: simulation of the bar + the axisymmetric potential. Third column: slow-bar + the axisymmetric potential. Fourth column: simulation of the full model (spiral arms + Galactic bar + axisymmetric potential).  $\Delta L_z$  is in units of  $\text{kpc} \times v_c$ , with  $v_c = 220 \text{ km s}^{-1}$ . The vertical lines mark the positions of the ILR (dashed), CR (solid), and the OLR (dotted) of the spiral pattern (red) and the bar (black). The color map indicates the number of particles  $\log(n)$ .

### 3.2 Radial migration by the bar

We explore now the isolated effect of the bar in the MW-like model. Proceeding as in the previous case, we measure  $\Delta L_z$  as a function of the initial radii for each particle within a period of time of  $\Delta t = 1 \text{ Gyr}$ . As shown in the upper second column panel of Figure 2, these changes occur along the stellar disc, linked to the bar resonances, as with the spiral pattern case; in this scenario, the distribution of  $\Delta L_z$  vs  $R_i$  is different from the spiral arms case, first, because the bar is a more massive structure, but mostly because of the greater pattern speed.

Although the ILR and CR of the bar are quite close, the distributions of  $\Delta L_z$  associated with each of them are still distinguishable. Note how particles outside OLR spread out, a similar but larger effect than the one seen with the spiral arms. This effect is mainly heating due to the OLR in both the bar and the spiral arms cases, as predicted by SB02. Note also that in the spiral arms case, the scatter in  $\Delta L_z$  develops around and beyond the OLR (as predicted theoretically), but in the bar case, the scatter starts a little beyond the OLR. This might be due to the diminishing surface gravity of the disc with the galactocentric distance. However, from the color map in Figure 2, it can be seen that the number of scattered particles is actually very small; a deeper study of this effect will be presented in a future work.

Again, by measuring the changes in orbital eccentricity, we can establish which part of the diagram  $\Delta L_z$  vs  $R_i$  represents radial heating or radial migration. From Figure 2 (second column, bottom panel), it is clear that around the ILR and beyond the OLR radial heating predominates because at these regions the stars modify their angular momentum by changing their orbital eccentricity. On the other hand, note how changes in eccentricity diminish as moving from the ILR to CR; the bimodality in the  $\Delta L_z$  distribution around CR of the bar implies that stars can change their radii by several kiloparsecs without heating their orbits.

#### 3.2.1 Slower Bar

As mentioned in the previous section, changes in angular momentum occur mainly around the resonances of the bar. As in the previous case,  $\Delta L_z$  around the ILR heats the orbits by changing considerably its eccentricity. On the other hand,  $\Delta L_z$  around CR is quite large but with small changes in the orbital eccentricities around that region. These two different outcomes for similar changes in angular momentum allow us to distinguish between radial heating and radial migration.

However, although a pattern speed of  $\Omega = 45 \text{ km s}^{-1} \text{ kpc}^{-1}$  is a common estimate for the MW bar, this value sets CR in close proximity to the ILR and it is not very clear what happens around CR. As an illustrative example we ran a simulation with a slower bar:  $\Omega = 20 \text{ km s}^{-1} \text{ kpc}^{-1}$  (the same used for the spiral arms).

Figure 2 shows also the two simulations with the bar-only model: one with a pattern speed of  $\Omega = 45 \text{ km s}^{-1} \text{ kpc}^{-1}$  (second column), the other with  $\Omega = 20 \text{ km s}^{-1} \text{ kpc}^{-1}$  (third column). First, notice that with a smaller pattern speed the separation between the ILR and CR increases; consequently, it is clearer what changes in angular momentum are linked to a given resonance. Around the ILR, the slow bar exchanges angular momentum with a substantial amount of heating, as seen by the changes in eccentricity. Meanwhile, there is a distinctive feature, around CR, in  $\Delta L_z$  of the slow bar with small changes in orbital eccentricity, as expected for radial migration; however, these changes are much smaller than those around CR of the faster bar, they even are smaller than the ones in the spiral-only model with the same pattern speed. This is mainly because, although the exchange of angular momentum is linked to resonances, in particular to CR, the bar (or spiral) should reach physically that given radius in order to accelerate the particles towards itself. Therefore, a faster bar, with CR located at a small radius, is efficient exchanging angular momentum

with the stellar disc through radial migration when compared with a slow bar, for which CR is well outside.

### 3.3 The Full Galactic Model (bar + spiral arms)

By isolating the effect of the spiral arms and the bar, we were able to better distinguish radial heating and radial migration induced by each non-axisymmetric structure, as well as their zones of influence within the disc. Now, the test particle disc is evolved in a full MW galactic model that includes both a bar and spiral arms. Top right panel of Figure 2 shows  $\Delta L_z$  in a period of time of  $\Delta t = 1$  Gyr.

Compared to the previous cases  $\Delta L_z$  is larger in magnitude and more spread throughout the disc. The resonance positions are indicated in Figure 2; at inner radii there is an overlapping of resonant regions, specifically the ILR of the bar and the ILR of the arms, which enhances the gains and losses of angular momentum when compared with the individual effect of either one.

With this study it is possible to elucidate whether resonance overlapping preserves the eccentricity and induces radial migration (Minchev & Famaey 2010; Minchev et al. 2011), or instead it only heats up the disc. Figure 2 (bottom right panel), shows the changes in orbital eccentricity in the period of time  $\Delta t$ . Note that within the region of resonance overlapping the diagram is dominated by substantial changes in eccentricity, i.e., the redistribution of angular momentum at this zone is not produced by radial migration, but preferentially by radial heating. This occurs because the resonances in that region are the ILR of the bar and the ILR of the arms, each of which is related to radial heating. Additionally, since these resonances are close to the CR of the bar, they reduce the radial migration that could be induced by CR.

On the other hand, the CR of the spiral pattern is located at a large radius where no resonance overlapping is present; consequently, the redistribution of angular momentum around the CR of the arms (as seen in top left panel of Figure 2) is preserved, even in the presence of the bar, and it can still be classified as radial migration because changes in orbital eccentricity are small.

Concerning the model with bar + transient spiral arms, we found that the changes in angular momentum are similar in magnitude to the ones in the model with steady arms, however those pervade on a large region (several kiloparsecs) of the disc; it is of little interest to present the same plot as Figure 2, since for the same period of time it would represent arms with constant speed, and when we plot the full 5 Gyr it just looks like a blurred image of Figure 2. In the next section we plot the initial radii distributions along the stellar disc, which are more suitable to study the cumulative effect on radial migration by both kinds of spiral arms (transient and steady).

Summarising, the bar and spiral arms, separately, induce radial heating and radial migration, and their zones of influence over the disc can be determined. When both structures are present: at inner radii, the radial mixing of the stellar disc is produced by the joint action of the perturbations and it is dominated by radial heating; while at outer radii, the redistribution of angular momentum is caused mostly by the spiral arms and dominated by radial migration. This

leads to an important conclusion: the imprint of the spiral arms may be identified even in the presence of the bar.

## 4 LINKING THE MDF TO THE INITIAL RADII DISTRIBUTION

Using the results of Section 3, we will now demonstrate that the spiral arms are able to present a characteristic signature of their existence in observations.

### 4.1 Initial radii distribution modelled with the different Galactic components

By comparing the experiments presented previously we can identify, from a theoretical point of view, the effect that the spiral arms and/or the bar drive into the radial mixing of the stellar disc, whether this is done by means of radial heating or radial migration, and the regions where it takes place.

Observationally speaking, it is not plausible to identify the radial migration occurring in the Galaxy through plain kinematics of stars. To do this it is necessary to add chemical labels to the stars. Former work on radial migration, including chemical evolution of the disc, predicts that a consequence of this mechanism is a flattening of the metallicity gradient (Schönrich & Binney 2009). However, this prediction might not be enough to confirm the presence of radial migration in the stellar disc (Sánchez-Blázquez et al. 2014).

Using a sample of red giants from the SDSS-III/APOGEE Data Release 12, in their Figure 5, Hayden et al. (2015), discovered new signatures of radial migration by measuring the MDF of stars from inner to outer radii in the MW; they found a change of shape of the MDF: a negatively skewed distribution at inner radii that changes to be positively skewed at large galactocentric radii. Using a simple model that includes radial migration, Hayden et al. (2015) are able to reproduce the observed MDF. This observed behaviour, and the interpretation of the change in shape of the MDF as radial migration, was later found in N-Body+SPH simulations by Loebman et al. (2016).

Taking a different approach, employing test particle simulations within a controlled observationally motivated model of the Galaxy, we find the same evidence for radial migration, but as we demonstrated in the sections above, our approach has the advantage of being able to isolate the effect of each perturber. In this manner, we endeavour to distinguish, at each Galactic radius, whether the shape of the MDF is due to the bar, the spiral arms or both.

Since a star preserves information of the state of the ISM at its birth place and epoch, the trend in the MDF skewness due to radial migration is reflected directly on the initial radii distribution. Therefore, instead of working with the MDF, we equivalently will employ the initial radii distribution of stars in our simulations, as a tracer of chemical abundance (note that small radii correspond to large chemical abundance in our scheme).

Figure 3 shows the initial radii distributions, i.e., the number of stars with a given initial galactocentric radius (at 0 Gyr) that at the end of the simulation (at 5 Gyr) are located within any of the different coloured bins, between  $3 < R < 13$  kpc. For purposes of comparison, in the top panel we plot together the distributions obtained with the three

Galactic models that we have used so far. In the three models the skewness of the distribution is reversed when going from inner to outer galactocentric radii, as expected from radial migration, but the asymmetry is more pronounced with the model that holds both bar and spiral arms.

Complementary to the conclusions of Section 3.3, the comparison of the initial radii distribution, showed in top panel of Figure 3, offers a new method to diagnose the perturber that induces the radial displacements of stars at each radius.

First note that, at the inner disc, the initial radii distribution produced by each perturber does not resemble that of the full model, meaning that both are important in shaping the MDF in this part of the Galaxy. Around the solar radius the distributions produced by the three models are quite similar, therefore one could be inclined to say it is impossible to determine which one is more influential, but with the precision achieved with this kind of models one can see that for the full model the inner tail of the curve is closer to that found when only the bar is considered, showing that in this region the effect of the bar is more important than that of the spiral arms. Finally at large galactocentric radii, there is a change in the skewness of the distribution, making the effect of the full model much more similar to the model with only the spiral arms. This means that at large radii, the MDF of the disc would be mainly shaped by the radial migration driven by the arms, with little influence from the bar.

Differences in the shapes of the tails for different models can potentially be observed with a large enough dataset, allowing to set restrictions for the structural and/or dynamical parameters of the non-axisymmetric structures of the MW.

The time interval to compute the diagram in Figure 3 is 0 – 5 Gyr. To ensure that neither the distinction between models nor the sign of the skewness for the distributions (in Figure 3) is due to short-period transient features, in Appendix A, we computed the initial radii distributions for two additional time frames. There we find that the models are distinguishable independently of the chosen time-frame. This strengthens the significance of the differences between models as well as our main conclusion: that the spiral arms can leave a distinguishable imprint on the MDF, even in the presence of the bar.

#### 4.2 Full model with transient spiral arms

Radial stellar migration is expected to be more efficient in the presence of transient spiral patterns (SB02). We have also implemented the full Galactic model with spiral arms growing and vanishing in a transient and smooth fashion, emerging each time with a decreasing pattern speed, going from 25 down to 17 km s<sup>-1</sup> kpc<sup>-1</sup> (for a complete description of the transient spiral arms model, see Section 2.2.1).

The bottom panel of Figure 3 shows the initial radii distributions for the simulation of the full model (Bar + long-lived arms) compared to the model of Bar + Transient arms. Note that as a consequence of the changing pattern speed, the distributions are modified at all radii when comparing with the case of long-lived arms. Also the peak of the distribution around the solar vicinity is slightly displaced towards a smaller radius, this is translated to a solar neighbourhood MDF with a peak near or slightly over solar metallicity.

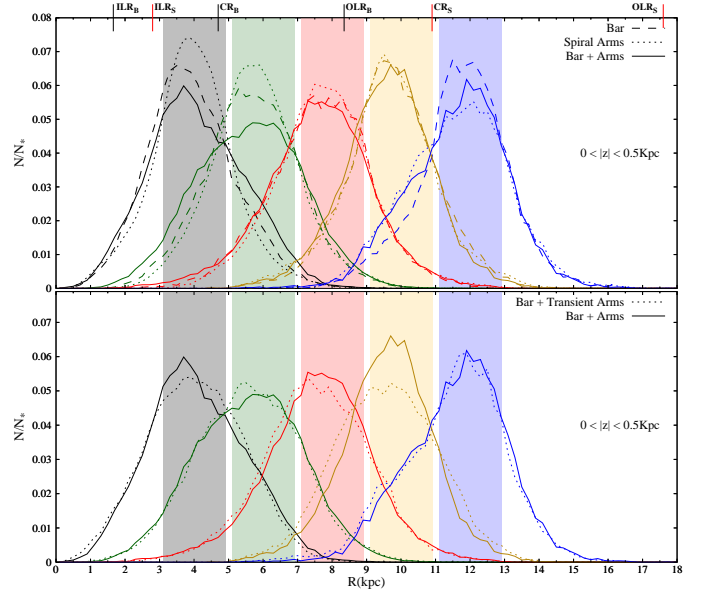


**Figure 3.** Initial galactocentric radii distribution of stars that at the end of the simulation are located within one of the five coloured bins. Each curve corresponds to the closest same-colour shaded bin.  $N$  is the number of stars at a given initial radius and  $N_*$  is the total number of stars that have ended within each coloured bin. Top: distributions for the three models; Spiral Arms (dotted), Bar (dashed), and Bar+Arms (solid). Vertical lines at top mark the positions of the ILR, CR, and the OLR for the spiral pattern and the bar. Bottom: distributions for the models Bar + long-lived Arms (solid) and Bar + transient Arms (dotted).

Meanwhile at outer radii the number of stars that migrate from the inner disc to the two outer bins is increased in the case of the bar + transient arms model; i.e., a transient spiral pattern would take more metal rich stars to the outer disc, causing in this region a more extended high-metallicity MDF tail, populated by stars that were born in the inner Galaxy.

The shape of the initial radii distributions induced by transient spiral arms, and its consequences to the MDF, are in good agreement with the APOGEE observations (Hayden et al. 2015). In fact these observations, that provide new evidence for radial migration, could be used to set constraints on chemo-dynamical Galactic models, through this we could even obtain an insight of the long-lived or transient nature of the spiral arms, or of the structural parameters of the spiral arms in a given galaxy, particularly in the MW (in a future work we will present a related study).

## 5 DISCUSSION

Through controlled test particle simulations in an observationally motivated detailed model of the MW, we isolate and compare the radial mixing in three different models: axisymmetric + spiral, axisymmetric + bar, axisymmetric + spiral + bar (full model). With this study we are able to distinguish whether a region of the disc is affected by either of the perturbers or by its joint action.

For the full model, the kinematics that arms and bar imprint to the stars suggest that at inner radii (less than



approximately 5 kpc for the angular speeds in our model) the radial mixing of the stellar disc is dominated by the joint action of the perturbers and it is constituted mainly by radial heating. At outer radii (beyond approximately 9 kpc) the redistribution of angular momentum is driven mainly by the spiral arms and dominated by radial migration. The exact details of the influence region of each structure depends on the structural and dynamical details of the model such as, masses, angular velocities, etc.

Radial migration leaves an imprint on the MDFs of the stellar disc; also transient spiral arms slightly enhance radial mixing and the skewness of the MDF when compared with long-lasting spiral arms; the exact shape of the MDF depends on the specific characteristics of the Galaxy. Comparison of the results of models with the DR12 from APOGEE can place new constraints on the details of structural and dynamical parameters of the spiral arms.

The MDF in the inner region of the disc is shaped by the action of both bar and spiral arms, while at outer radii the MDF is mainly shaped by the spiral arms. With this work we demonstrate that the spiral arms show an specific signature readily identifiable on the MDFs. More work is needed to fully fit the APOGEE MDFs.

Our approach does not consider the chemical abundance nor its evolution, instead we are employing the initial galactic position as a proxy for metallicity. However, the similarities obtained between our models and the observed MDF curves of the Milky Way Galaxy, show the relevance of the galactic potential in shaping the MDFs curves; additionally, the difference in the MDFs between the three models presented here prove that the specific potential employed to model the Galaxy is vital.

## 6 CONCLUSIONS

With the use of a very detailed fully adjustable potential, to better represent the Milky Way Galaxy—to the best of our observational knowledge—we performed simulations to study radial migration and to approximate the metallicity distribution function to elucidate the importance of the non-axisymmetric components of the Galaxy (bar and spiral arms). With this model we are able to split the contribution of different galactic components to a given phenomenology.

We are able to separate the effect of the bar and spiral arms on radial heating and radial migration as well as their zones of influence over the disc; when both structures are present, the radial mixing of the stellar disc at inner radii is produced by the joint action of the perturbers, and it is dominated by radial heating. At outer radii, the redistribution of angular momentum is caused mostly by the spiral arms and dominated by radial migration. This means that the imprint of the spiral arms may be identified even in the presence of the strong influence of the massive bar.

Similarly, the MDF in the inner region of the disc is shaped by the action of both bar and spiral arms, while at outer radii the MDF is mainly shaped by the spiral arms.

This study offers a new method to diagnose the large scale non-axisymmetric structure that induces radial displacements of stars at each radius.

The spiral arms present a characteristic signature of their existence in observations, particularly on the radial

migration and heating, which directly relates to the shape of the MDF as seen by APOGEE.

Our approach does not consider the chemical abundance nor its evolution, instead we employ the initial galactic position as a proxy for metallicity. Based on the similarities of our results to the MDF curves in the Galaxy we can state confidently that the specific gravitational potential is of great importance to reproduce them.

## ACKNOWLEDGEMENTS

We thank the anonymous referee for a careful reading and several excellent suggestions. We acknowledge DGTIC-UNAM for providing HPC resources on the Cluster Supercomputer Miztli. L.A.M.M and B.P. acknowledge DGAPA-PAPIIT through grants IN-114114 and IG-100115, L.A.M.M and E.M. acknowledge DGAPA-PAPIIT through grant IN105916. A.P. acknowledges DGAPA-PAPIIT through grant IN-109716. L.A.M.M. acknowledges support from a DGAPA-UNAM postdoctoral fellowship.

## APPENDIX A: SKEWNESS OF THE INITIAL RADII DISTRIBUTION AT DIFFERENT TIME-FRAMES

In Figure A1 we show the initial radii distributions for the time frames 0–2 Gyr (Top) and 2–4 Gyr (bottom). In both panels, the three models are still distinguishable from each other in the same manner as was seen in Figure 3 (top panel); also, notice that for this new set of distributions the skewness keeps changing in sign when going from inner to outer radii (as it does in Figure 3). This confirms that the results in Section 4 are real rather than an artefact, showing that the spiral arms can potentially leave its imprint, through radial migration, on the observable properties of the Milky Way's disc.

## REFERENCES

- Agertz, O., Teyssier, R., & Moore, B. 2011, MNRAS, 410, 1391
- Allen C., Santillán A., 1991, Rev. Mex. Astron. Astrofis., 22, 255
- Antoja, T., Valenzuela, O., Pichardo, B., et al. 2009, ApJL, 700, L78
- Antoja T. et al., 2014, A&A, 563, A60
- Aumer, M., Binney, J., & Schönrich, R. 2016, arXiv:1604.00191
- Baba, J., Saitoh, T. R., & Wada, K. 2013, ApJ, 763, 46
- Benjamin R. A. et al., 2005, ApJL, 630, L149
- Bird, J. C., Kazantzidis, S., & Weinberg, D. H. 2012, MNRAS, 420, 913
- Blum R. D., 1995, ApJL, 444, L89
- Buta R., Vasylyev S., Salo H., Laurikainen E., 2005, AJ, 130, 506
- Calchi Novati, S., de Luca, F., Jetzer, P., Mancini, L., & Scarpetta, G. 2008, A&A, 480, 723
- Churchwell, E., Babler, B. L., Meade, M. R., et al. 2009, PASP, 121, 213
- Combes F., Sanders R. H., 1981, A&A, 96, 164
- Dehnen, W. 2000, AJ, 119, 800
- Drimmel R., 2000, A&A, 358, L13
- Drimmel, R., & Spergel, D. N. 2001, ApJ, 556, 181
- Dwek E. et al., 1995, ApJ, 445, 716
- Edvardsson, B., Andersen, J., Gustafsson, B., et al. 1993, A&A, 275, 101



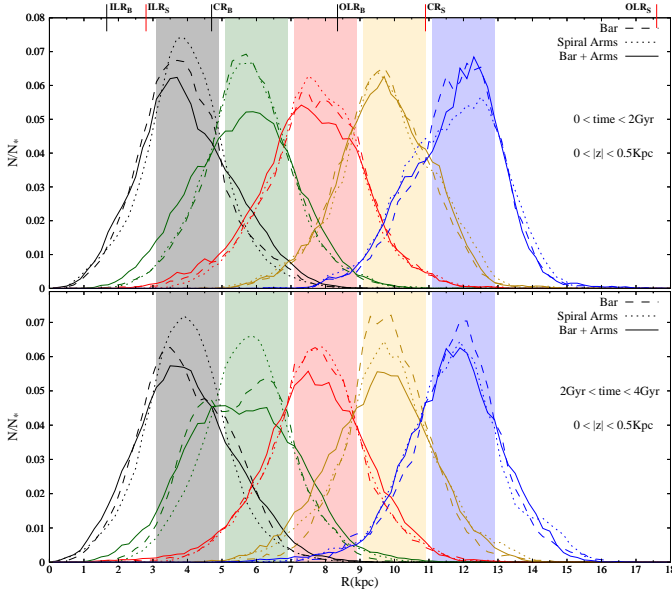


**Figure A1.** Top: initial galactocentric radii distribution of stars that at  $t_f = 2$  Gyr are located within one of the five coloured bins. Bottom: same as top but for  $t_f = 4$  Gyr. In both panels, each curve corresponds to the closest same-colour shaded bin.  $N$  is the number of stars at a given initial radius, and  $N_*$  is the total number of stars that have ended within each coloured bin. Vertical lines at the top axis mark the positions of the ILR, CR, and the OLR for both the spiral pattern and the bar.

Pettitt, A. R., Dobbs, C. L., Acreman, D. M., & Bate, M. R. 2015, *MNRAS*, 449, 3911  
 Pichardo, B., Moreno, E., Allen, C., et al. 2012, *AJ*, 143, 73  
 Pichardo, B., Martos, M., & Moreno, E. 2004, *ApJ*, 609, 144  
 Rautiainen, P., & Salo, H. 1999, *A&A*, 348, 737  
 Roca-Fàbrega, S., Valenzuela, O., Figueras, F., et al. 2013, *MNRAS*, 432, 2878  
 Roškar, R., Debattista, V. P., Quinn, T. R., Stinson, G. S., & Wadsley, J. 2008, *ApJL*, 684, L79  
 Roškar, R., Debattista, V. P., Quinn, T. R., & Wadsley, J. 2012, *MNRAS*, 426, 2089  
 Sanders R. H., Tubbs A. D., 1980, *ApJ*, 235, 803  
 Saha, K., & Elmegreen, B. 2016, arXiv:1607.01953  
 Sánchez-Blázquez, P., Rosales-Ortega, F. F., Méndez-Abreu, J., et al. 2014, *A&A*, 570, A6  
 Sellwood, J. A. 2011, *MNRAS*, 410, 1637  
 Sellwood J. A., Binney J. J., 2002, *MNRAS*, 336, 785  
 Sellwood, J. A., & Carlberg, R. G. 1984, *ApJ*, 282, 61  
 Sellwood, J. A., & Carlberg, R. G. 2014, *ApJ*, 785, 137  
 Schönrich, R., & Binney, J. 2009, *MNRAS*, 396, 203  
 Stanek K. Z., Udalski A., Szymański M., KaLuZny J., Kubiak Z. M., Mateo M., Krzemiński W., 1997, *ApJ*, 477, 163  
 Vera-Ciro, C., D'Onghia, E., Navarro, J., & Abadi, M. 2014, *ApJ*, 794, 173  
 Weiner B. J., Sellwood J. A., 1999, *ApJ*, 524, 112  
 Wilson, T. L., & Rood, R. 1994, *ARA&A*, 32, 191  
 Zhao H., 1994, PhD thesis, Columbia Univ.  
 Zhao, H. 1996, *MNRAS*, 283, 149

Freudenreich H. T., 1998, *ApJ*, 492, 495  
 Gerhard O., 2011, *MSAIS*, Vol. 18, 185  
 Gerhard O., 2002, in Da Costa G. S., Jerjen H., eds, *ASP Conf. Ser. 273, The Dynamics, Structure & History of Galaxies: A Workshop in Honour of Professor Ken Freeman*. Astron. Soc. Pac. (San Francisco, CA: ASP), p. 73  
 Grand, R. J. J., Kawata, D., & Cropper, M. 2012, *MNRAS*, 421, 1529  
 Grand, R. J. J., Kawata, D., & Cropper, M. 2012, *MNRAS*, 426, 167  
 Halle, A., Di Matteo, P., Haywood, M., & Combes, F. 2015, *A&A*, 578, A58  
 Hayden, M. R., Bovy, J., Holtzman, J. A., et al. 2015, *ApJ*, 808, 132  
 Henry, R. B. C., & Worthey, G. 1999, *PASP*, 111, 919  
 Hernquist L., 1993, *ApJS*, 86, 389  
 Hockney, R. W., & Brownrigg, D. R. K. 1974, *MNRAS*, 167, 351  
 Kent S. M., 1992, *ApJ*, 387, 181  
 Loebman, S. R., Debattista, V. P., Nidever, D. L., et al. 2016, *ApJL*, 818, L6  
 Martinez-Medina, L. A., Pichardo, B., Pérez-Villegas, A., & Moreno, E. 2015, *ApJ*, 802, 109  
 Martos, M., Hernandez, X., Yáñez, M., Moreno, E., & Pichardo, B. 2004, *MNRAS*, 350, L47  
 Mata-Chávez, M. D., Gómez, G. C., & Puerari, I. 2014, *MNRAS*, 444, 3756  
 Minchev, I., & Famaey, B. 2010, *ApJ*, 722, 112  
 Minchev, I., Famaey, B., Combes, F., et al. 2011, *A&A*, 527, A147  
 Minchev, I., Chiappini, C., & Martig, M. 2013, *A&A*, 558, A9  
 Minchev, I., Chiappini, C., & Martig, M. 2014, *A&A*, 572, A92  
 Moreno, E., Pichardo, B., & Schuster, W. J. 2015, *MNRAS*, 451, 705  
 Pichardo, B., Martos, M., Moreno, E. & Espresate, J., 2003, *ApJ*, 582, 230